Efficient Aero-Structural Wing Optimization Using Compact Aerofoil Decomposition

D.J. Poole *, C.B. Allen †, T.C.S. Rendall‡

Department of Aerospace Engineering, University of Bristol, Bristol, BS8 1TR, U.K.

Aerodynamic shape optimization of an aero-structural transonic wing is presented using a compact set of design variables. Modal decomposition (via singular value decomposition) of a training library of aerofoils to extract a compact set of aerofoil design variables has previously been shown to be highly effective. These have been used for high-fidelity global optimization of aerofoils. Hence, this work applies these design variables to optimization of an aero-structural wing. A representative transonic aircraft wing with defined structural modes is optimized as a rigid and aeroelastic shape. For fixed planform optimization, using as few as nine variables at ten spanwise sections is enough permit shock-free solutions when using a gradient-based optimizer for both the rigid and aeroelastic shapes. A drag reduction of 21.7% of the rigid wing is obtained. However, the aero-structural solution of the optimised rigid wing shows a shocked solution, demonstrating the need to consider the optimization of the aeroelastic shape. As such, optimization of the aeroelastic wing is considered, where a drag reduction of and 29.7% is obtained against the aeroelastic baseline wing.

I. Introduction and Background

The design of an aircraft is inherently an exercise in the coupling and subsequent compromise of multiple, and often independent, disciplines. Nowhere is this more apparent than in the design of aircraft wings, where the aerodynamic performance typically dominates, but where the design is dictated by the behaviour of many other disciplines. Multi-disciplinary analysis (MDA) is the framework that proceeds when analysis of each discipline is integrated into an overall coupled system. Furthermore, beyond analysis, the overall multi-disciplinary system may be linked to an optimization process leading to the multi-disciplinary optimization (MDO) framework [1].

Commonly, engineering optimization problems embed high-fidelity computational analysis into the process, which is used to determine various metrics against which to optimise. The problem then reduces to that of finding the optimum design (often a geometric problem) that optimises a cost function subject to constraint functions. The cost and constraint functions typically rely on outputs from the analysis. An optimization algorithm is then required to link the analysis to the design process, where the algorithm uses values of the cost and constraints to determine a vector of design variables that link to changes in the design to hopefully improve the cost. A parameterization is the vehicle that governs how the design variables affect the design. An example single-discipline problem is finding the optimum aerodynamic aerofoil or wing shape to minimise drag subject to a constraint on lift, where a computational fluid dynamics (CFD) solver is used to determine the aerodynamic performance; see [2–7] for example.

In aircraft wing design, the aero-structural coupled system dominates the performance. When determining aerodynamic performance of the wing in flight, the static wing shape is deflected as aerodynamic loads are transferred to the structure and an equilibrium state results. Simulation of this system commonly requires coupling of separate CFD and computational structural mechanics (CSM) solvers in a partitioned manner [8–11]. This solution approach has the advantage of requiring little development of new codes, with the main development requirements being the solution coupling, and the force and displacement interpolation and

*Lecturer. AIAA Member. Email: d.j.poole@bristol.ac.uk

†Professor of Computational Aerodynamics. AIAA Senior Member. Email: c.b.allen@bristol.ac.uk

‡Lecturer. AIAA Member. Email: thomas.rendall@bristol.ac.uk

mesh deformation needed due to non-coincident fluid and structural meshes. The coupling requires that an outer iteration loop be added to march the solution to equilibrium. The interpolation and mesh deformation are often handled separately, but a unified approach using radial basis function (RBF) interpolation was shown to be highly effective [12]. A similar approach, but using B-spline-based methods, has also recently been presented [13]. An alternative solution approach is the monolithic method, where a single solver that solves the governing equations synchronously is developed [14, 15]. While accuracy and convergence tends to be better with the monolithic approach, the development costs are a barrier. For example, all four codes that submitted results to the aero-structural benchmarking case of the Sixth AIAA CFD Drag Prediction Workshop used a partitioned solution approach [16].

Once a suitable aero-structural solver is developed, full MDO of the wing that optimises for the performance of the coupled aerodynamic and structural responses can be realised. There exists a deep history of performing ever increasing fidelity of aero-structural optimization [17]. Due to the cost associated with aero-structural optimization, local gradient-based optimization algorithms have usually been the tool of choice. The problem then exists of determining the gradients of the cost and constraints with respect to the design variables. The adoption of the adjoint approach [18] permits all gradients of flow quantities with respect to surface changes to be evaluated for a computing cost that is similar to a single flow solution. Using this, coupled aero-structural adjoint methods have been presented [19–21], which has permitted high-fidelity, large-scale aero-structural optimization [22]. Furthermore, recent developments include the ongoing work to couple more disciplines into the process, including coupling aerodynamics, structures and acoustics in a fully coupled unsteady optimization of rotorcraft [23].

Large design variable problems permit detailed small-scale optimisation. However, the quantity of design variables has a significant effect on the convergence of the optimiser, as well as the definition of multimodality in the problem. Furthermore, while gradient-based methods are the most popular optimization algorithms in MDO, if alternatives (such as population-based) methods are to be exploited, then lower-dimensional design spaces become key. Dimensionality reduction techniques have become a useful approach for reducing the dimensionality associated with aerodynamic shape optimization. Of these, singular value decomposition-based approaches take a training matrix of data (for example a number of aerofoil shapes [24, 25]), and project a reduced-order basis approximation of the original data. Work by the authors has shown that this is a very efficient approach for producing a reduced set of aerofoil deformation modes [26] that are suitable for aerodynamic optimization of aerofoils [6] and wings [27]. The reduced set of modes has been used for high-fidelity global optimization of aerofoils [6]. Furthermore, comprehensive experiments [28] have shown singular value decomposition (SVD) modes to be the most efficient approach at representing a generic aerofoil compared to most other commonly used parameterization methods. Recent work by Li *et al.* [29] has also suggested this approach can allow for interactive aerofoil design.

The work presented in this paper extends the application of these modes further by considering high-fidelity aero-structural wing optimization. The overall goal of this work is to make high-fidelity global multi-disciplinary optimization of wings a reality, and the use of a compact aerofoil decomposition for the design variables is a pillar to this goal.

The remainder of the paper is organised as follows: the compact modal decomposition and how this is applied to wing optimization is outlined in section II; the solver and datum solution is presented in section III; the optimization problem and chosen optimizer is presented in section IV; results and analysis is given in section V; conclusions are given in VI.

II. Decomposition for Wing Design Variables

The design variables used in the optimization process are the weightings of various sectional deformations. These sectional deformations come about by performing a matrix decomposition that uses SVD on a training library of aerofoils. The resulting modes represent a reduced basis projection of the full-basis aerofoil design space, however, the SVD also produces a reduced-basis projection that is the most efficient way of representing the full-basis space. Full wing deformations are separable into sectional and planform deformations, which is also performed here. The aerofoil deformation modes from the SVD are applied sectionally, then planform deformations are applied. The full process of obtaining and applying these deformations are described below.

II.A. SVD for Sectional Deformations

To obtain aerofoil deformation modes, a training library of aerofoils needs to first be collated. The selection of the training library is one of the most important steps in this process since the characteristics of the library map to the characteristics of the deformation modes. The authors have previously published work [26] that used a metric-based filtering approach to select the training library. In this work, the library of aerofoils is as previously used by the authors for transonic aerofoil optimization [6]. The aerofoil data was obtained from the UIUC database[a], and was subsequently smoothed and re-parameterised to ensure consistency.

A training library contains M aerofoils each parameterised with N surface points, where the i-th surface point of the m-th aerofoil has coordinates (x_{i_m}, z_{i_m}). To obtain aerofoil deformation modes, the vector difference between each surface point of all aerofoils is computed. The vector difference of the i-th surface point between the m-th and n-th aerofoils is given as $(\Delta x_{i_{m,n}}, \Delta z_{i_{m,n}})$, and this is stacked into a single vector:

$$[\Delta x_{1_{m,n}}, \ldots, \Delta x_{N_{m,n}}, \Delta z_{1_{m,n}}, \ldots, \Delta z_{N_{m,n}}]^T$$

Hence, this process produces $M_{def} = M(M-1)/2$ deformation vectors, which are collated into a single deformation matrix that has $2N$ rows and M_{def} columns:

$$\boldsymbol{\Psi} = \begin{pmatrix} \Delta x_{1_{1,2}} & \cdots & \Delta x_{1_{1,M}} & \Delta x_{1_{2,3}} & \cdots & \Delta x_{1_{M-1,M}} \\ \vdots & \ddots & \vdots & \vdots & \ddots & \vdots \\ \Delta x_{N_{1,2}} & \cdots & \Delta x_{N_{1,M}} & \Delta x_{N_{2,M}} & \cdots & \Delta x_{N_{M-1,M}} \\ \Delta z_{1_{1,2}} & \cdots & \Delta z_{1_{1,M}} & \Delta z_{1_{2,3}} & \cdots & \Delta z_{1_{M-1,M}} \\ \vdots & \ddots & \vdots & \vdots & \ddots & \vdots \\ \Delta z_{N_{1,2}} & \cdots & \Delta z_{1_{1,M}} & \Delta z_{N_{2,M}} & \cdots & \Delta z_{N_{M-1,M}} \end{pmatrix}$$

The deformation matrix has an SVD given by:

$$\boldsymbol{\Psi} = \mathbf{U}\boldsymbol{\Sigma}\mathbf{V}^T \tag{1}$$

where $\mathbf{U}$ is an orthonormal $2N \times 2N$ matrix, $\boldsymbol{\Sigma}$ is a diagonal matrix with $\min\{2N, M_{def}\}$ diagonal entries arranged in descending order, and $\mathbf{V}^T$ is an orthonormal $M_{def} \times M_{def}$ matrix. The columns of $\mathbf{U}$ contain the aerofoil deformation modes, and these are extracted column-wise and used for the optimization. The diagonal entries of $\boldsymbol{\Sigma}$ contain the singular values, which may be used to determine now much 'energy' each mode has to the overall system.

The use of the SVD here is for geometric filtration of the high-degree training matrix into a low-degree representation use deformation modes. To do this, the first D modes (i.e. first D columns of U) may be extracted and a D-rank approximation of the original matrix may be obtained by:

$$\boldsymbol{\Psi} \approx \boldsymbol{\Psi}^{(D)} = \widetilde{\mathbf{U}}\widetilde{\boldsymbol{\Sigma}}\widetilde{\mathbf{V}}^T \tag{2}$$

where the tilde is used to denote reduced forms of the SVD matrices. Once a low-rank approximation is found through SVD, the following is true [30]:

$$\|\boldsymbol{\Psi} - \boldsymbol{\Psi}^{(D)}\|_F \leq \|\boldsymbol{\Psi} - \boldsymbol{\Phi}\|_F \tag{3}$$

where $\boldsymbol{\Phi}$ is any matrix of rank D and $\|\cdot\|_F$ is the Frobenius norm. Hence, the error between the low-rank approximation and the full rank approximation will always be at least as good as the error between any other k-rank matrix and the full-rank matrix. In this sense, the SVD produces an optimal low order projection of the higher dimensional space into the lower dimensional one. The first four deformation modes are shown in figure 1 (these are superimposed on NACA0012 for visualisation purposes). It is clear to see that the first mode represents a thickness change, then the second represents a camber change, indicating that for this library of aerofoils, these are the two most important aerofoil design parameters respectively.

[a] http://m-selig.ae.illinois.edu/ads/coord_database.html

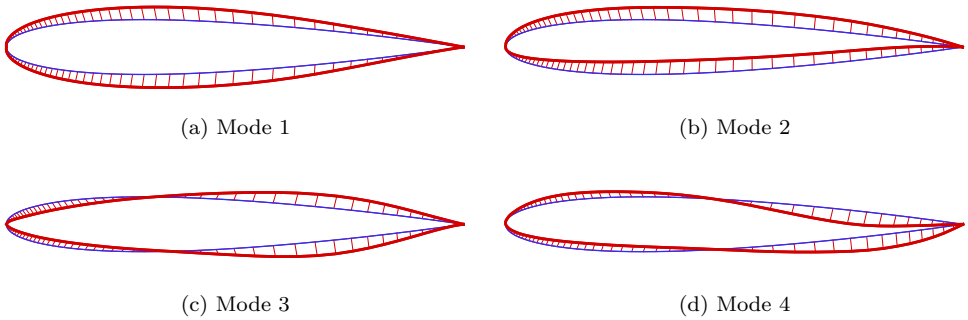

(a) Mode 1 (b) Mode 2

(c) Mode 3 (d) Mode 4

Figure 1: First four aerofoil deformation modes (superimposed on NACA0012 for visualisation)

Given the required number of deformation modes, D, in the optimization, the design variables are the weightings of each deformation mode. The overall deformation is then a linear superposition of each mode:

$$\mathbf{\Delta X} = \sum_{i=1}^{D} \alpha_i \mathbf{U}_i \tag{4}$$

where α_i is the design variable relating to the i-th mode and $\mathbf{U}_i$ is the i-th mode, which is the i-th column of $\mathbf{U}$.

II.B. Application to Wing Deformation

The aerofoil deformation modes are surface deformations, however, to ensure body-fitted meshes are retained in the optimization the mesh also needs to deform. Furthermore, the surface deformation modes are applied sectionally, which is defined here.

The sectional deformations are applied at a fixed number of spanwise stations, i.e. equation 4 is applied at these stations locally, and ten are used in this work. However, the sectional deformations can also be applied in a global nature, and while this is not as flexible as local deformation, the authors have shown global deformations to provide reasonable optimization results but at a fraction of the cost [27]. The sectional deformations are applied using the RBF control point approach, where a set of control points are defined in the fluid domain and global volume interpolation translates deformation of the control points to deformation of the aerodynamic mesh. Hence, the modal deformations are used to drive deformation of the control points that subsequently deform the wing surface and mesh. These deformations are decoupled, so the control point modal deformations are determined off-line and then applied in the optimization process.

At the heart of this technique in an RBF interpolation developed originally for aero-structure coupling and mesh motion by Rendall and Allen [12]. An RBF interpolation, s, is a linear combination of basis functions, whose argument is the Euclidean distance, $\|\cdot\|$ between the point to be interpolated in the domain, $\mathbf{x}$, and the N points in the known data set. Therefore, the influence that a known point has is controlled by a function, ϕ, that depends on the distance from the interpolated point:

$$s(\mathbf{x}) = \sum_{i=1}^{N} \beta_i \phi(\|\mathbf{x} - \mathbf{x}_i\|) + p(\mathbf{x}) \tag{5}$$

Control points decouple the shape deformations from the surface mesh and provide a unified framework for surface and mesh deformation. Given n_c control points, a global RBF interpolation of this nature provides exact recovery of data at known sites, and interpolation of that data away from the sites. In the case of optimization, the data to be interpolated is deformation of the control points, hence a deformation field is created. The position of the aerodynamic mesh points in the field therefore defines the deformation of those points. Since exact recovery of data at the know sites (in this case the position of the control points, which for the j-th control point is defined as $(x_{c_j}, y_{c_j}, z_{c_j})$) is specified, the interpolation takes the form:

$$\Delta \mathbf{x}_c = \mathbf{M}\boldsymbol{\beta}^x$$

where

$$\Delta \mathbf{x}_c = \begin{pmatrix} \Delta x_{c_1} \\ \vdots \\ \Delta x_{c_{n_c}} \end{pmatrix} \qquad \boldsymbol{\beta}^x = \begin{pmatrix} \beta_1^x \\ \vdots \\ \beta_{n_c}^x \end{pmatrix} \qquad \mathbf{M} = \begin{pmatrix} \phi_{1,1} & \cdots & \phi_{1,n_c} \\ \vdots & \ddots & \vdots \\ \phi_{n_c,1} & \cdots & \phi_{n_c,n_c} \end{pmatrix}$$

and analogous definitions hold for the y and z coordinates. The radial basis function $\phi_{i,j} = \phi(\|\mathbf{x}_{c_i} - \mathbf{x}_{c_j}\|)$ can take a number of forms, but the radially-decaying functions of Wendland [31] are a good choice for the mesh deformation problem to give the interpolation a local character and ensure deformation is contained in a region near the moving body. The C^2 function is used here.

Once the linear system is solved, the resulting deformation field can be evaluated at the location of each mesh point. The deformation of an aerodynamic mesh point is given by:

$$\Delta x_a = \sum_{i=1}^{n_c} \beta_i^x \phi(\|\mathbf{x}_{c_i} - \mathbf{x}_a\|) \tag{6}$$

with analogous definitions for y and z.

Using RBF interpolation has the advantage of being able to specify the level of control since control points can be placed arbitrarily in, on the boundary, or outside the fluid domain. For example, figure 2 shows two different set-ups for the control points. However, irrespective of the location of the control points, modal deformations defined on the aerofoil surface may not be coincident with the control points so control point deformations must be defined. The authors [32] showed a number of techniques for achieving this, and an inverse RBF interpolation is an effective approach. However, if the aerodynamic surface and control points are coincident, the modal deformations are sampled at the control point sites and used directly.

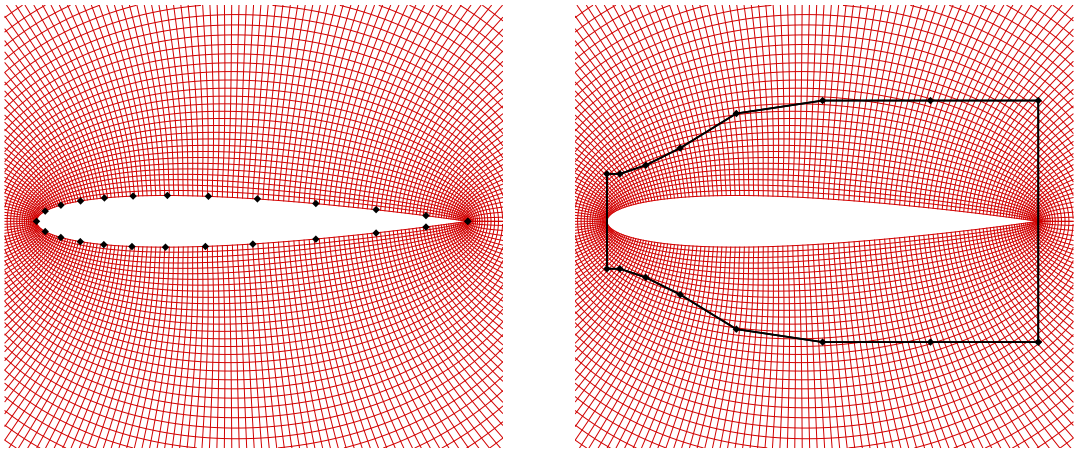

Figure 2: Example of two different locations of control points

The set-up of control points around the wing used in this paper (see below) is shown in figure 3. Modal deformations are applied sectionally at ten spanwise station (on the red control points), while intermediate control points are used to permit smooth spanwise deformations between the deformation slices. The deformation of blue points uses a partition of unity-blend of the deformation slices at either side. A trigonometric function is used. The control point cage is transformed to the local wing coordinates. For example, figure 3 shows the cage around both a rigid wing and a deformed wing. Hence, the sequences of operations is given a set of design variables, $\boldsymbol{\alpha}$, sectional deformations at the ten spanwise stations occurs (equation 4). The intermediate sectional deformations are then calculated. Once all control point deformations are defined and calculated, mesh deformation occurs.

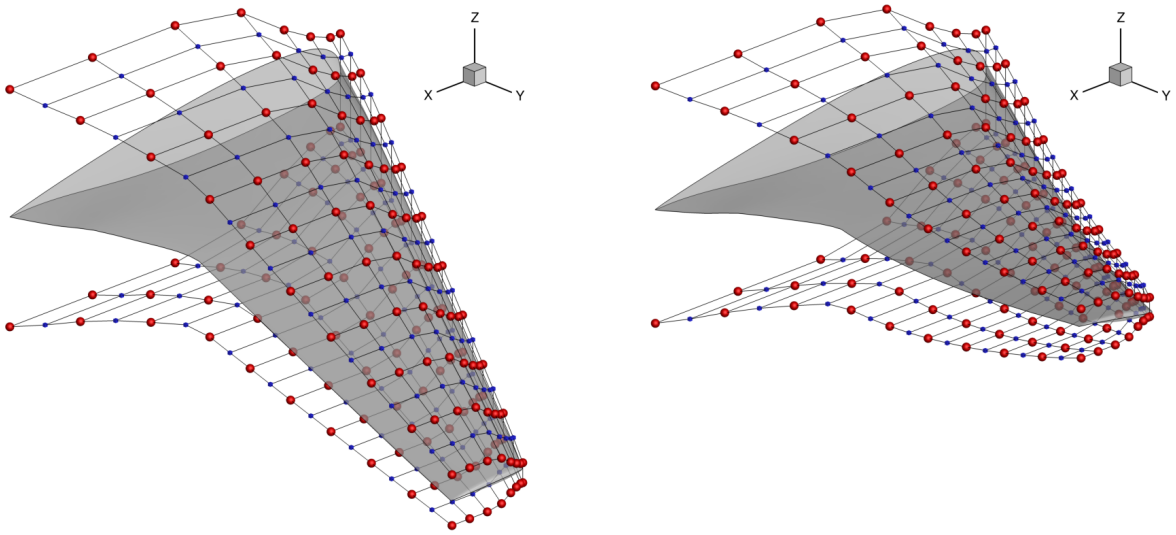

Figure 3: Control point cages around rigid and aeroelastic wing

III. Aero-structural Solver and Case Definition

The aero-structural solver is based on the structured multiblock solver of Allen [33, 34], with the coupled solver added through the work of Rendall and Allen [12]. In the case considered in this work, the flow is governed by the Euler equations, which are solved using finite volume integration with the Jameson-Schmidt-Turkel scheme [35]. Convergence acceleration is achieved through multigrid [34]. A modal structural solver is applied where coupling between the aerodynamic and structural grids, and subsequent mesh motion, is achieved through RBF coupling [12] that uses a reduced point cloud between aerodynamic and structural neighbour nodes [36]. Strong coupling of the two systems is employed for dynamic calculations. Newmark temporal integration [37] is used to march the solution.

To demonstrate using the compact aerofoil decomposition for aero-structural optimization, the MDO wing [38, 39] is used, where the structural model and associated structural mode shapes are defined. Figure 4 shows the MDO wing planform. Also shown is the aerodynamic surface mesh and the structural grid. For the aerodynamic mesh, a 400,000 node, eight-block structured C-mesh was generated [40] which has a 129 $\times$ 65 surface mesh, 25 nodes on either side of the wake, and 25 nodes between the inner and outer boundary. Figure 5 shows the block structure and the near-field mesh. A 2515 node wing-box structural model is used with the modes defined in Haase *et al.* [39]

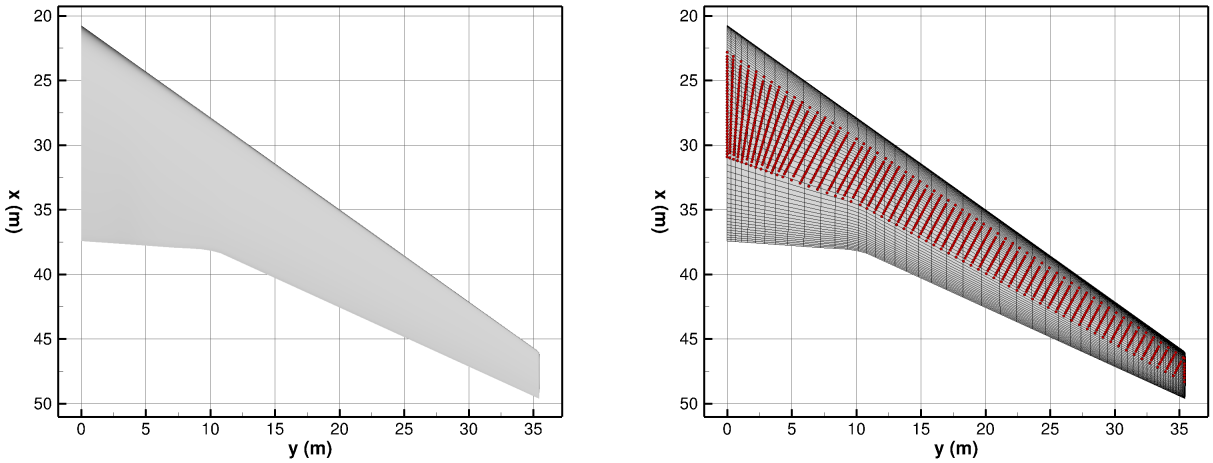

Figure 4: MDO Wing and meshes in planform view

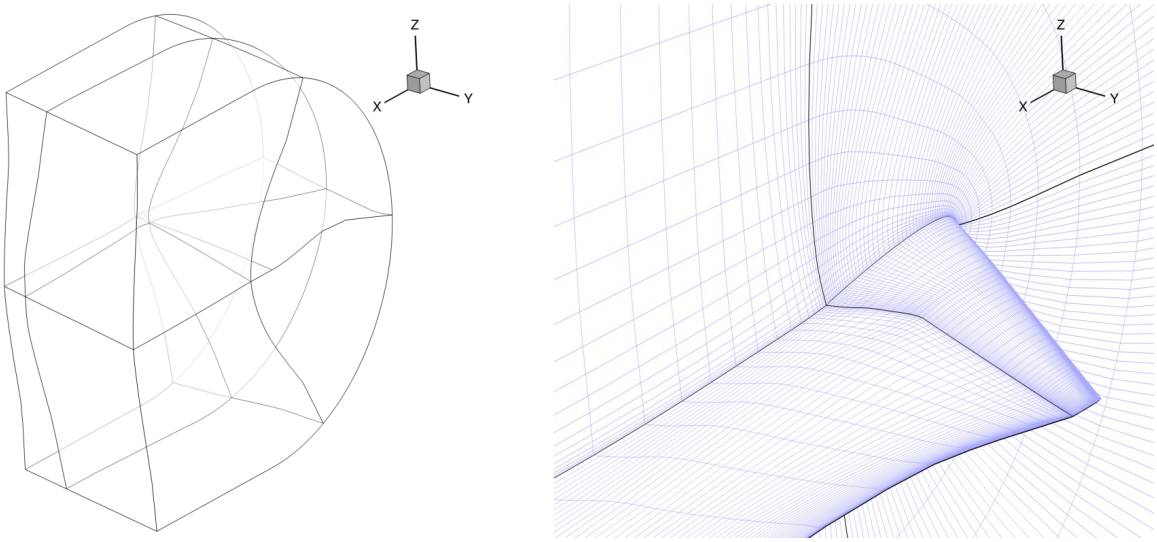

Figure 5: Block structure and near-field mesh planes

Throughout this work, a trimmed cruise condition of $C_L = 0.4$ at $M_\infty = 0.85$ is used. Unless otherwise stated, all wings are trimmed to this condition. The MDO wing has 18 defined structural modes and all are used for this work. Using fewer structural modes makes almost no difference to the convergence of the system and to the run-time of the solver. Hence, As such, to ensure an accurate solution, the full 18 prescribed modes are used.

The performance metrics of the rigid and aeroelastic MDO wing are given in table 1, while surface pressure contours are given in figure 6. The aeroelastic wing clearly offloads outboard and shifts load inboard, resulting in an overall lower root bending moment. However, this produces an overall drag penalty.

Table 1: Forces of rigid and aeroelastic MDO wing

	C_L	C_D	C_{M_x}	C_{M_y}	Δz_{tip}
Rigid	0.4	0.0157	0.184	-0.481	0.0m
Aeroelastic	0.4	0.0179	0.144	-0.386	6.16m

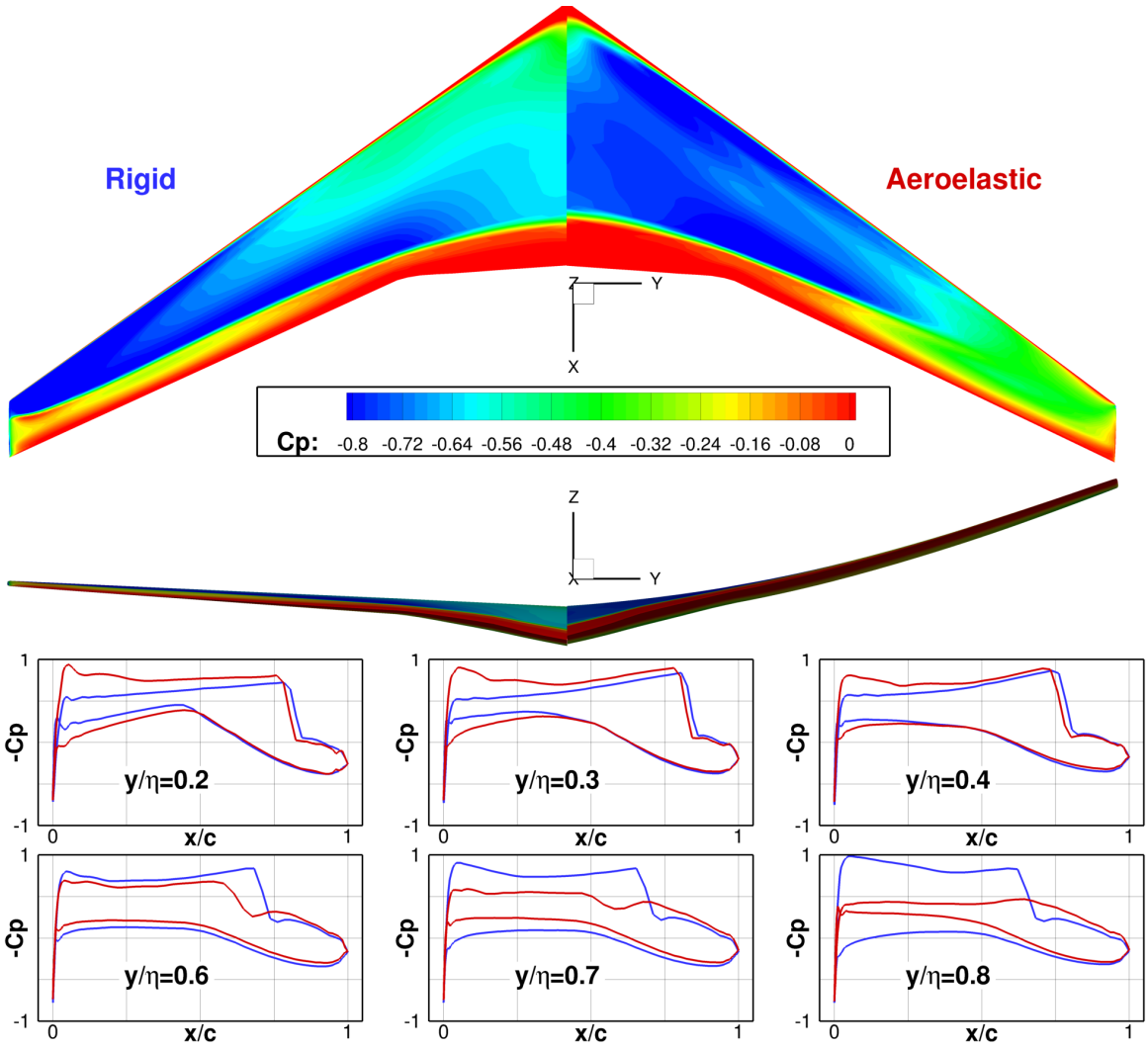

Figure 6: Surface C_P of rigid and aeroelastic wing shapes

IV. Optimization Problem and Algorithm

A generic single-objective optimization problem optimizes a cost function, J, which is a function of a vector of D design variables, $\boldsymbol{\alpha}$, subject to a vector of inequality constraints, $\mathbf{g}$, and equality, $\mathbf{h}$, constraints. The problem considered in this paper is aerodynamic shape optimization. The objective is drag minimization subject to constraints on lift, C_L and internal volume V. The problem is given by:

$$\begin{aligned} \underset{\boldsymbol{\alpha}\in\Re^D}{\text{minimise}} \quad & C_D \\ \text{subject to} \quad & C_L \geq 0.4 \\ & V \geq V(\text{initial}) \end{aligned} \tag{7}$$

The design variables of the problem are nine aerofoil deformation modes applied at ten equally spaced sections across the span of the wing. Each mode at each section is a different design variable and results in 90 variables. Furthermore, to allow induced drag to reduce, a linear (root-to-tip) twist variable is used, and to allow balance of the lift loading, angle of attack is also a design variable. This results in 92 design variables.

Using structural modal analysis is an effective means to determine the coupled aero-structural performance of the wing. However, when used in an optimization process, the primary assumption is that modifying the aerodynamic shape has minimal effect on the structural response. This assumption holds assuming the

structure is not changed, and since a wing-box is modelled and no planform changes occur, this is reasonable.

In the case considered in this paper, the overall goal of this work is to permit large-scale global aeroelastic shape optimization. Global optimization is particularly useful when the design space is known to be multimodal, and the overall goal is to locate the globally optimal solution. In the first instance, only sectional changes are considered and since fixed planform wing optimization is generally considered to be unimodal (to within numerical tolerances) [41], a gradient-based sequential quadratic programming (SQP) optimizer (which solves non-linear constrained optimization problems) is used. Future work will consider planform changes, where global optimization algorithms become necessary. The chosen optimizer is the Sparse Nonlinear Optimizer (SNOPT) [42].

The gradient-based optimizer requires the sensitivities of the cost and constraint functions with respect to each design variable at each major iteration. For this work, a second-order finite difference stencil is used so for each design variable, two extra flow solutions are required (one each for the positive and negative perturbations) to evaluate the sensitivities. For computational efficiency, a parallel decomposition of the gradient evaluation is employed such that each design design variable sensitivity is assigned to its own CPU, which handles the geometry (and CFD volume mesh) deformations and flow solutions. Once the gradients are evaluated, these are passed back to the master process where the optimizer update occurs.

V. Wing Optimization Results

For this work, two optimization cases are consider. Case I involves the optimization of the rigid MDO wing at the trimmed cruise flight condition ($C_L = 0.4$ at $M_\infty = 0.85$). Case II then involves the static optimization of the aeroelastic MDO wing at the trimmed cruise flight condition. Hence, both cases are static optimizations (flow only), but with the aeroelastic solver used to define the aeroelastic deformation.

V.A. Case I: Optimization of rigid MDO wing

Table 2 gives the optimization results of case I, which is the static optimization of the rigid MDO wing, while figure 7 gives the convergence of the optimizer. Both constraints are satisfied and the drag has reduced substantially. Figure 8 shows the surface pressures of the baseline and optimized wings, and demonstrates that the result is shock-free at the design condition. Since this problem is inviscid, the two primary sources of drag are wave drag and induced drag. As the problem is shock-free, wave drag has been substantially reduced. Induced drag is reduced through the use of twist, and as can be seen in the aerofoil stacks in figure 9, the wing has been twisted. Otherwise, relatively small changes to the aerofoil sections have occurred.

Table 2: Optimization results of case I - rigid MDO wing

	C_L	C_D	C_{M_x}	C_{M_y}	ΔC_D
Initial	0.4	0.0157	0.184	-0.481	-
Optimized	0.4	0.0123	0.173	-0.470	**-21.7%**

The static rigid optimizations have produced the expected shock-free result at the design condition, however, it is interesting to see how this wing performs under aeroelastic loading. Hence, the case I optimized wing is run with the structural model to determine the aeroelastic solution. Table 3 gives the force coefficients of the aeroelastic MDO wing and the aeroelastic solution of the optimized rigid wing, while figure 10 shows the surface pressure coefficients. Figure 11 show the wing shapes. It should be noted that all wings are trimmed to $C_L = 0.4$. Clearly the aeroelastic solution of the optimized rigid wing has a shock structure, with a single shock at the inboard and outboard sections, and a double shock midspan and this has resulted in an overall drag increase. Also, the extra outboard load of the rigid optimised wing has resulted in a lower tip deflection. It is well known that single-point drag minimization produces highly optimised point-design solutions with poor off-design performance [43], so this trend is not surprising. However, this does suggest that perhaps performing static optimization of the MDO wing aeroelastic shape could mitigate this.

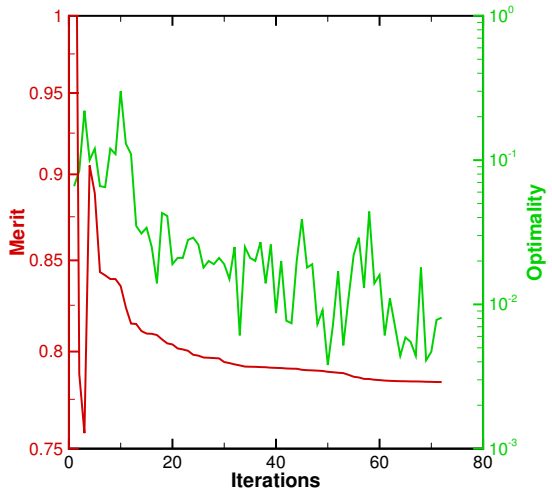

Figure 7: Optimizer convergence of case I

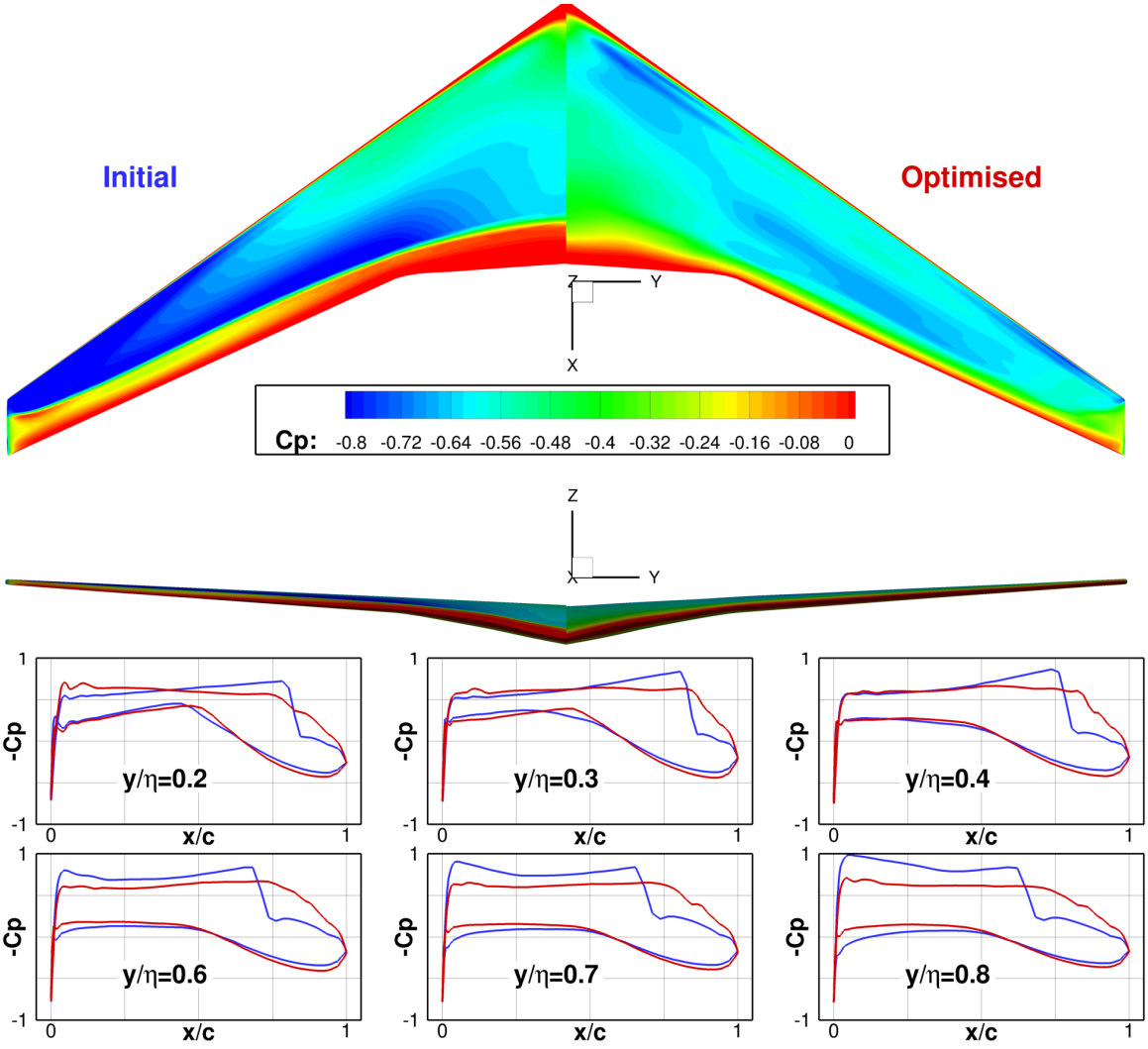

Figure 8: Surface C_P of initial and optimised wing shapes for case I

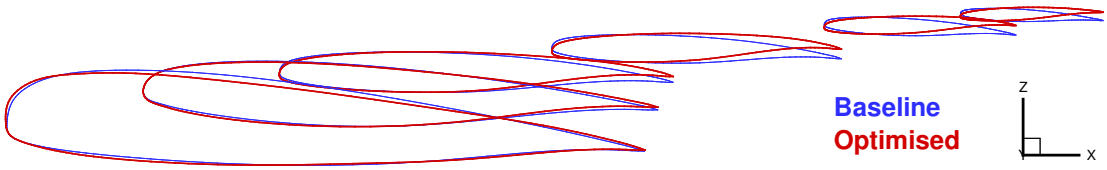

Figure 9: Aerofoil stacks of initial and optimised wing shapes for case I

Table 3: Forces of aeroelastic MDO wing and aeroelastic solution of optimised rigid wing

	C_L	C_D	C_{M_x}	C_{M_y}	Δz_{tip}
MDO	0.4	0.0179	0.144	-0.386	6.16m
Optimised	0.4	0.0193	0.130	-0.368	4.94m

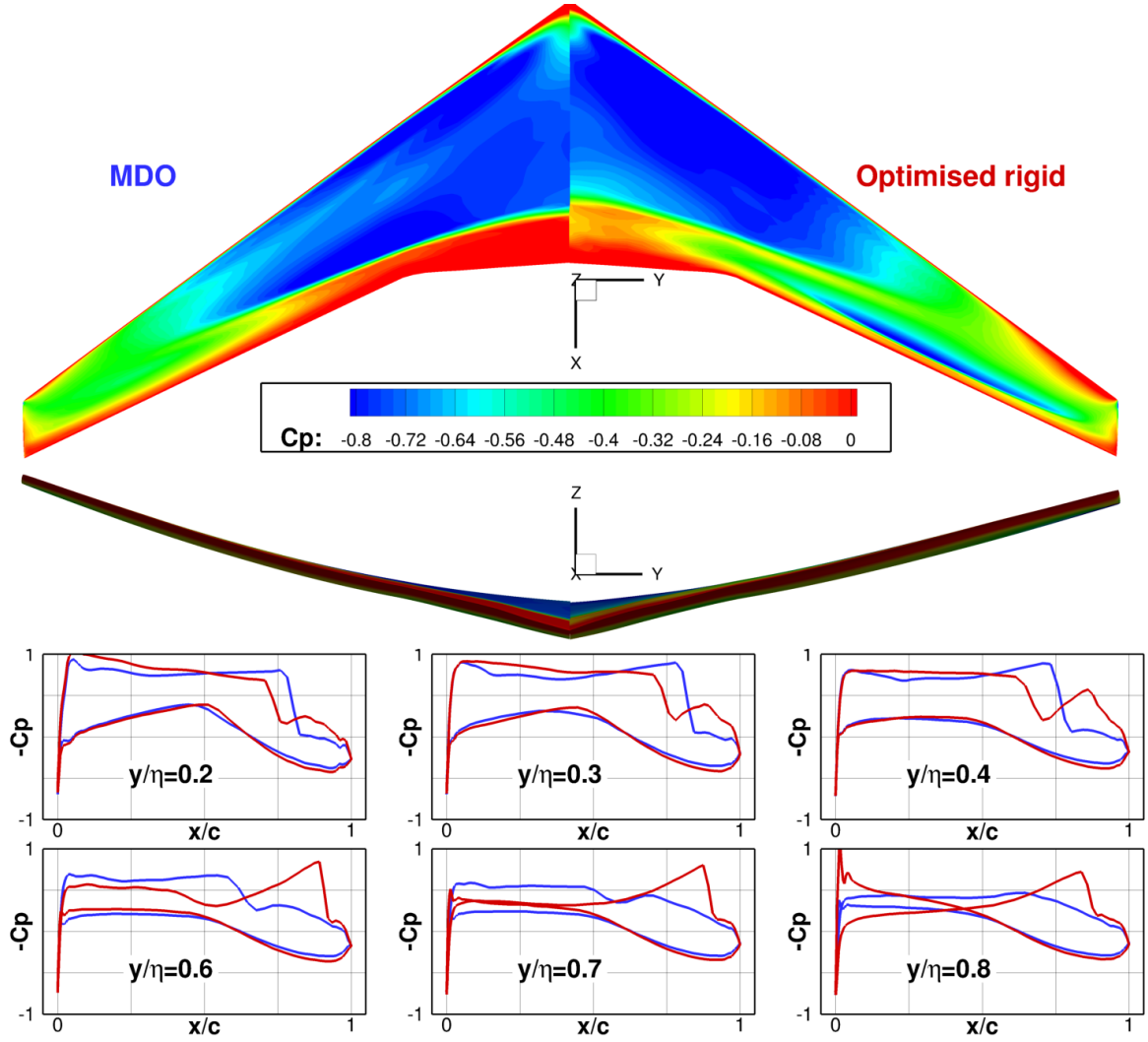

Figure 10: Surface C_P of MDO wing and case I result under aeroelastic loading

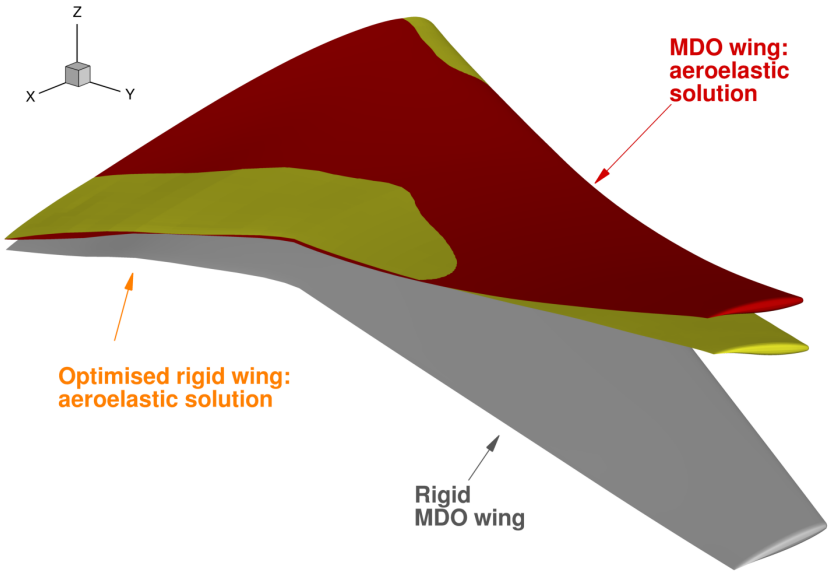

Figure 11: Comparison of rigid and aeroelastic MDO wing shapes, and case I result wing under aeroelastic loading

V.B. Case II: Optimization of aeroelastic MDO wing shape

The second case is the optimization of the aeroelastic MDO wing shape. For this case, the aeroelastic solver was run to convergence to obtain the aeroelastic wing shape. Aerodynamic shape optimization was then performed on that aeroelastic wing shape. Table 4 gives the optimization results while figure 12 shows the optimizer convergence. As in case I, the optimizer has reduced drag substantially while the two constraints are active. Figure 13 gives the surface pressures, showing a shock-free solution being achieved. Furthermore, while not being considered in the optimizations, the moment coefficients show an interesting trend. In case II, the root bending moment has increased, indicating that load has been shifted outboard (this is also shown in the surface pressures).

Table 4: Optimization results of case II - aeroelastic MDO wing

	C_L	C_D	C_{M_x}	C_{M_y}	ΔC_D
Initial	0.4	0.0179	0.143	-0.386	-
Optimized	0.4	0.0126	0.177	-0.432	**-29.7%**

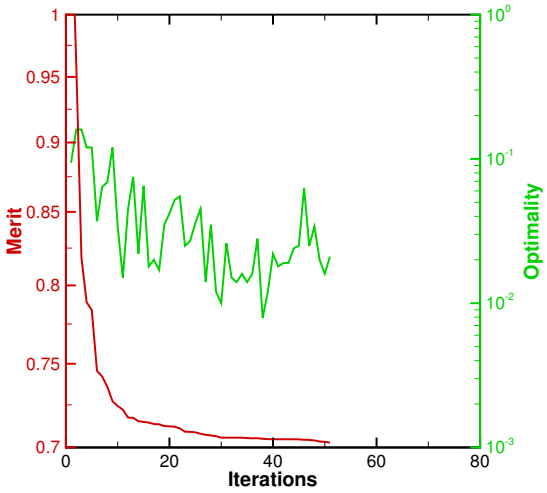

Figure 12: Optimizer convergence of case II

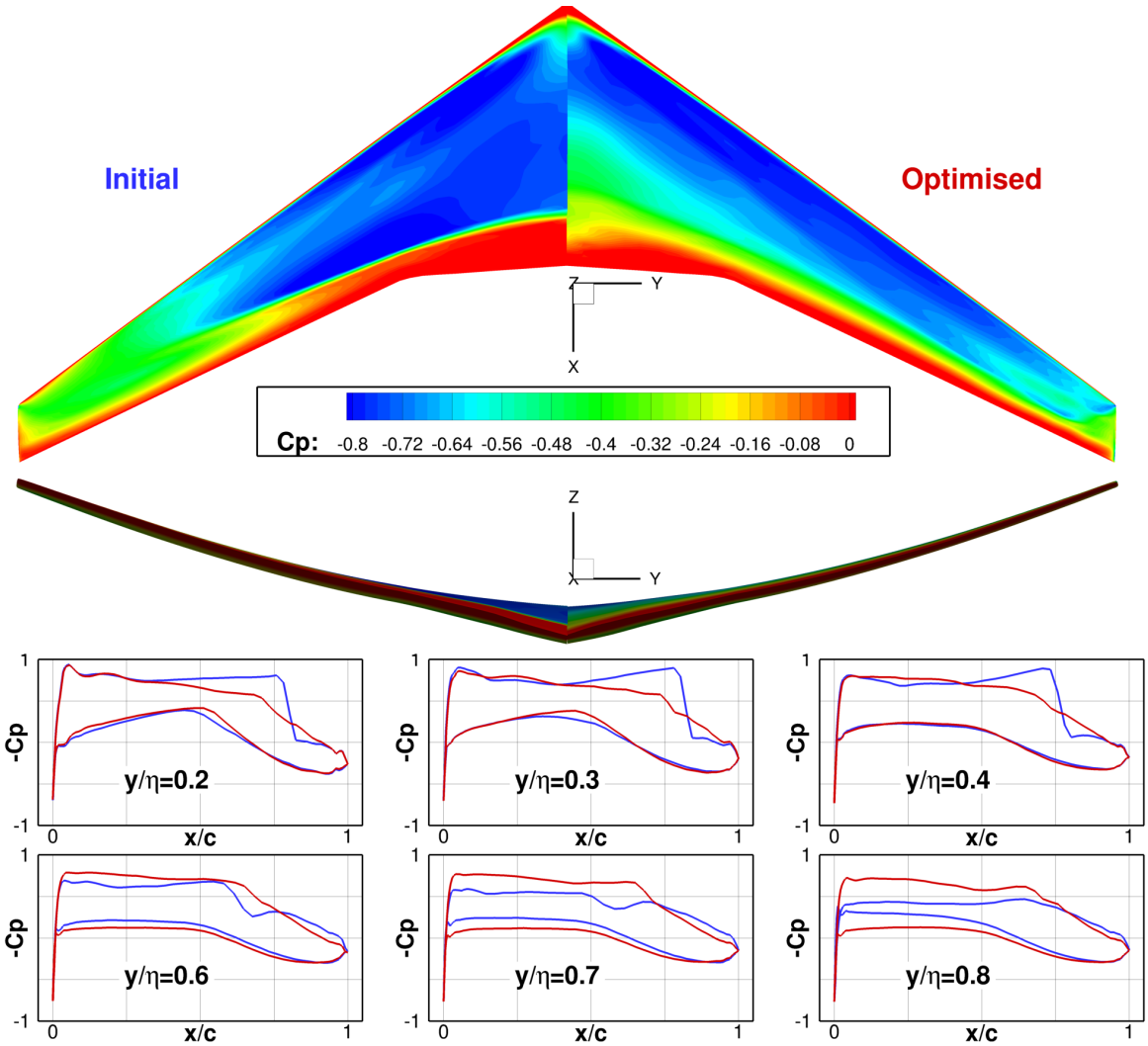

Figure 13: Surface C_P of initial and optimised wing shapes for case II

VI. Conclusions

Low-dimensional, efficient multi-disciplinary optimization is presented for aero-structural wing optimization. While much aero-structural optimization work to date has considered high-fidelity, many-variable problems, little work has considered the possibility of reducing the dimensionality of the problem. Lower-dimensionality problems often have positive effects on the convergence of the optimization algorithm as well as possibly laying the foundations for the use of population-based global algorithms. As such, the authors have previously presented an efficient method for determining aerofoil deformations via singular value decomposition. These have been shown to provide a highly efficient set of design variables for optimization. Hence, in this paper, these are being applied to multi-disciplinary optimization. This work considers these for fixed planform drag minimization as proof-of-concept that these modes can be applied within a multi-disciplinary optimization framework.

The compact aerofoil design variables are applied sectionally for inviscid drag minimization subject to lift and internal volume constraints. Two cases are investigated, with the first being drag minimization of a rigid wing in transonic flow and the second being optimization of an aeroelastic solution. Shock-free solutions were demonstrated for both cases, demonstrating the effectiveness of this reduced set of design variables for optimization. Hence, this approach can help introduce global optimization methods (where a reduced set of design variables is important) into the multi-disciplinary optimization process. Future work will consider this.

References

[1] Martins, J. R. R. A. and Lambe, A. B., "Multidisciplinary Design Optimization: A Survey of Architectures," *AIAA Journal*, Vol. 51, No. 9, 2013, pp. 2049–2075.
doi:10.2514/1.J051895.

[2] Hicks, R. M. and Henne, P. A., "Wing Design by Numerical Optimization," *Journal of Aircraft*, Vol. 15, No. 7, 1978, pp. 407–412.
doi:10.2514/6.1977-1247.

[3] Qin, N., Vavalle, A., Le Moigne, A., Laban, M., Hackett, K., and Weinerfelt, P., "Aerodynamic Considerations of Blended Wing Body Aircraft," *Progress in Aerospace Sciences*, Vol. 40, No. 6, 2004, pp. 321–343.
doi:10.1016/j.paerosci.2004.08.001.

[4] Morris, A. M., Allen, C. B., and Rendall, T. C. S., "CFD-based Optimization of Aerofoils Using Radial Basis Functions for Domain Element Parameterization and Mesh Deformation," *International Journal for Numerical Methods in Fluids*, Vol. 58, No. 8, 2008, pp. 827–860.
doi:10.1002/fld.1769.

[5] Allen, C. B. and Rendall, T. C. S., "Computational-Fluid-Dynamics-Based Optimisation of Hovering Rotors Using Radial Basis Functions for Shape Parameterisation and Mesh Deformation," *Optimization and Engineering*, Vol. 14, 2013, pp. 97–118.
doi:10.1007/s11081-011-9179-6.

[6] Poole, D. J., Allen, C. B., and Rendall, T. C. S., "High-fidelity aerodynamic shape optimization using efficient orthogonal modal design variables with a constrained global optimizer," *Computers & Fluids*, Vol. 143, 2017, pp. 1–15.
doi:10.1016/j.compfluid.2016.11.002.

[7] Poole, D. J., Allen, C. B., and Rendall, T. C. S., "Global Optimization of Wing Aerodynamic Optimization Case Exhibiting Multimodality," *Journal of Aircraft*, Vol. 55, No. 4, 2018, pp. 1576–1591.
doi:10.2514/1.C034718.

[8] Geuzaine, P., Brown, G., Harris, C., and Farhat, C., "Aeroelastic Dynamic Analysis of a Full F-16 Configuration for Various Flight Conditions," *AIAA Journal*, Vol. 41, No. 3, 2003, pp. 363–371.
doi:10.2514/2.1975.

[9] Taylor, N. V., Allen, C. B., Gaitonde, A., and Jones, D. P., "A structure-coupled CFD method for time-marching flutter analysis," *The Aeronautical Journal*, Vol. 108, No. 1086, 2004, pp. 389–401.
doi:10.1017/S0001924000000208.

[10] Woodgate, M. A., Badcock, K. J., Rampurawala, A. M., Richards, B. E., Nardini, D., and deC Henshaw, M. J., "Aeroelastic calculations for the Hawk aircraft using the Euler equations," *Journal of Aircraft*, Vol. 42, No. 4, 2005, pp. 1005–1011.
doi:10.2514/1.5608.

[11] Sanchez, R., Palacios, R., Economon, T. D., Kline, H. L., Alonso, J. J., and Palacios, F., "Towards a Fluid-Structure Interaction solver for problems with large deformations within the open-source SU2 suite," *57th AIAA/ASCE/AHS/ASC Structures, Structural Dynamics, and Materials Conference*, San Diego, California, 2016, AIAA Paper 2016-0205.
doi:10.2514/6.2016-0205.

[12] Rendall, T. C. S. and Allen, C. B., "Unified Fluid-Structure Interpolation and Mesh Motion Using Radial Basis Functions," *International Journal for Numerical Methods in Engineering*, Vol. 74, No. 10, 2008, pp. 1519–1559.
doi:10.1002/nme.2219.

[13] Zhang, Z. J., Khosravi, S., and Zingg, D. W., "High-fidelity aerostructural optimization with integrated geometry parameterization and mesh movement," *Structural and Multidisciplinary Optimization*, Vol. 55, 2017, pp. 1217–1235.
doi:10.1007/s00158-016-1562-7.

[14] Michler, C., Hulshoff, S. J., van Brummelen, E. H., and de Borst, R., "A monolithic approach to fluid-structure interaction," *Computers & Fluids*, Vol. 33, No. 5-6, 2004, pp. 839–848.
doi:10.1016/j.compfluid.2003.06.006.

[15] Hübner, B., Walhorn, E., and Dinkler, D., "A monolithic approach to fluidstructure interaction using spacetime finite elements," *Computer Methods in Applied Mechanics and Engineering*, Vol. 193, No. 23-26, 2004, pp. 2087–2104.
doi:10.1016/j.cma.2004.01.024.

[16] Keye, S. and Mavriplis, D., "Summary of Data from the Sixth AIAA CFD Drag Prediction Workshop: Case 5 (Coupled Aero-Structural Simulation)," *55th AIAA Aerospace Sciences Meeting*, Grapevine, Texas, 2017, AIAA Paper 2017-1207.
doi:10.2514/6.2017-1207.

[17] Sobieszczanski-Sobieski, J. and Haftka, R. T., "Multidisciplinary aerospace design optimization: survey of recent developments," *Structural Optimization*, Vol. 14, No. 1, 1997, pp. 1–23.
doi:10.1007/BF01197554.

[18] Jameson, A., "Aerodynamic design via control theory," *Journal of Scientific Computing*, Vol. 3, No. 3, 1988, pp. 233–260.
doi:10.1007/BF01061285.

[19] Maute, K., Nikbay, M., and Farhat, C., "Coupled Analytical Sensitivity Analysis and Optimization of Three-Dimensional Nonlinear Aeroelastic Systems," *AIAA Journal*, Vol. 39, No. 11, 2001, pp. 2051–2061.
doi:10.2514/2.1227.

[20] Martins, J. R. R. A., Alonso, J. J., and Reuther, J. J., "A Coupled-Adjoint Sensitivity Analysis Method for High-Fidelity Aero-Structural Design," *Optimization and Engineering*, Vol. 6, No. 1, 2005, pp. 33–62.
doi:10.1023/B:OPTE.0000048536.47956.62.

[21] Kenway, G. K. W., Kennedy, G. J., and Martins, J. R. R. A., "Scalable Parallel Approach for High-Fidelity Steady-State Aeroelastic Analysis and Adjoint Derivative Computations," *AIAA Journal*, Vol. 52, No. 5, 2014, pp. 935–951.
doi:10.2514/1.J052255.

[22] Kenway, G. K. W. and Martins, J. R. R. A., "Multi-point High-fidelity Aerostructural Optimization of a Transport Aircraft Configuration," *Journal of Aircraft*, Vol. 51, No. 1, 2014, pp. 144–160.
doi:10.2514/1.C032150.

[23] Mavriplis, D., Fabiano, E., and Anderson, E., "Recent Advances in High-Fidelity Multidisciplinary Adjoint-Based Optimization with the NSU3D Flow Solver," *55th AIAA Aerospace Sciences Meeting*, Grapevine, Texas, 2017, AIAA Paper 2017-1669.
doi:10.2514/6.2017-1669.

[24] Toal, D. J. J., Bressloff, N. W., Keane, A. J., and Holden, C. M. E., "Geometric Filtration Using Proper Orthogonal Decomposition for Aerodynamic Design Optimization," *AIAA Journal*, Vol. 48, No. 5, 2010, pp. 916–928.
doi:10.2514/1.41420.

[25] Ghoman, S. S., Sarhaddi, D., Chen, P. C., Wang, Z., and Kapania, R. K., "A Hybird Optimization Strategy Using Design-Space Evolution and POD-based Order Reduction," *12th AIAA Aviation Technology, Integration and Operations (ATIO) Conference and 14th AIAA/ISSMO Multidisciplinary Analysis Optimization Conference*, Indianapolis, Indiana, 2012, AIAA Paper 2012-5631.
doi:10.2514/6.2012-5631.

[26] Poole, D. J., Allen, C. B., and Rendall, T. C. S., "Metric-Based Mathematical Derivation of Efficient Airfoil Design Variables," *AIAA Journal*, Vol. 53, No. 5, 2015, pp. 1349–1361. doi:10.2514/1.J053427.

[27] Allen, C. B., Poole, D. J., and Rendall, T. C. S., "Wing aerodynamic optimization using efficient mathematically-extracted modal design variables," *Optimization and Engineering*, Vol. 19, No. 2, 2018, pp. 453–477. doi:10.1007/s11081-018-9376-7.

[28] Masters, D. A., Taylor, N. J., Rendall, T. C. S., Allen, C. B., and Poole, D. J., "Geometric Comparison of Aerofoil Shape Parameterization Methods," *AIAA Journal*, Vol. 55, No. 5, 2017, pp. 1575–1589. doi:10.2514/1.J054943.

[29] Li, J., Bouhel, M. A., and Martins, J. R. R. A., "Data-Based Approach for Fast Airfoil Analysis and Optimization," *AIAA Journal*, Published online. doi:10.2514/1.J057129.

[30] Eckart, C. and Young, G., "The Approximation of One Matrix by Another of Lower Rank," *Psychometrika*, Vol. 1, No. 3, 1936, pp. 211–218. doi:10.1007/BF02288367.

[31] Wendland, H., *Scattered Data Approximation*, Cambridge University Press, 1st ed., 2005.

[32] Poole, D. J., Allen, C. B., and Rendall, T. C. S., "Optimal Domain Element Shapes for Free-Form Aerodynamic Shape Control," *53rd AIAA Aerospace Sciences Meeting*, Kissimmee, Florida, 2015, AIAA Paper 2015-0762. doi:10.2514/6.2015-0762.

[33] Allen, C. B., "Multigrid Convergence of Inviscid Fixed- and Rotary-Wing Flows," *International Journal for Numerical Methods in Fluids*, Vol. 39, No. 2, 2002, pp. 121–140. doi:10.1002/fld.282.

[34] Allen, C. B., "Parallel simulation of unsteady hovering rotor wakes," *International Journal for Numerical Methods in Engineering*, Vol. 68, No. 6, 2006, pp. 632–649. doi:10.1002/nme.1723.

[35] Jameson, A., Schmidt, W., and Turkel, E., "Numerical solution of the Euler equations by finite volume methods using Runge Kutta time stepping schemes," *14th Fluid and Plasma Dynamics Conference*, Palo Alto, California, 1981, AIAA Paper 1981-1259. doi:10.2514/6.1981-1259.

[36] Rendall, T. C. S. and Allen, C. B., "Reduced Surface Point Selection Options Efficient Mesh Deformation Using Radial Basis Functions," *Journal of Computational Physics*, Vol. 229, No. 8, 2010, pp. 2810–2820. doi:10.1016/j.jcp.2009.12.006.

[37] Newmark, N. M., "A Method of Computation for Structural Dynamics," *Journal of the Engineering Mechanics Division*, Vol. 85, No. 3, 1959, pp. 67–94.

[38] Allwright, S., "Reference aircraft performance and primary sensitivities," Tech. rep., 1997, Technical report D.3.12.R, MDO/TR/BAE/SA970530/1.

[39] Haase, D., Selmin, V., and Winzell, B., *Progress in Computational Flow-Structure Interaction*, Springer, chap. Notes on Numerical Fluid Mechanics and Multidisciplinary design, 2002.

[40] Allen, C. B., "Towards Automatic Structured Multiblock Mesh Generation using Improved Transfinite Interpolation," *International Journal for Numerical Methods in Engineering*, Vol. 74, No. 5, 2008, pp. 697–733. doi:10.1002/nme.2170.

[41] Yu, Y., Lyu, Z., Xu, Z., and Martins, J. R. R. A., "On the influence of optimization algorithm and initial design on wing aerodynamic shape optimization," *Aerospace Science and Technology*, Vol. 75, 2018, pp. 183–199.
doi:10.1016/j.ast.2018.01.016.

[42] Gill, P. E., Murray, W., and Saunders, M. A., "SNOPT: An SQP Algorithm for Large-Scale Constrained Optimization," *SIAM Journal on Optimization*, Vol. 12, No. 4, 2002, pp. 979–1006.
doi:10.1137/S1052623499350013.

[43] Poole, D. J., Allen, C. B., and Rendall, T. C. S., "Comparison of Point Design and Range-Based Objectives for Transonic Aerofoil Optimization," *AIAA Journal*, Vol. 56, No. 8, 2018, pp. 3240–3256.
doi:10.2514/1.J056627.